Journal of the

WATERWAYS, HARBORS AND COASTAL ENGINEERING DIVISION

Proceedings of the American Society of Civil Engineers

WAVE DIFFRACTION BY DETACHED BREAKWATER

By Michael Stiassnie[1] and Gedeon Dagan[2]

INTRODUCTION

A thin barrier of finite length in water of finite depth and infinite extent (Fig. 1) is considered herein. An incident gravity wave, attacking the obstacle from infinity, is deffracted and scattered by the thin barrier, which is a satisfactory representation of a detached breakwater of large length to thickness ratio. The aim of the present work is to compute the waves potential energy (i.e., the wave height) in the region surrounding the obstacle. The maps of the state of the sea near the barrier (Figs. 2 to 10) permit a sound evaluation of the breakwater performance and, therefore, an improved design.

The computations are carried out first for a monochromatic incident wave and an impervious obstacle. The solution is extended afterwards to the cases of a pervious barrier and a random incident wave.

The present solution is compared with Wiegel's (9) work on a barrier of semi-infinite length and with Morse and Rubenstein (5) study of scattering of electromagnetic waves.

BASIC EQUATIONS

As usual the flow is assumed to be inviscid and irrotational and velocity potential

$$\Phi(x,y,z,t) = \phi(x,y,z) \exp(-i\omega t) \quad (\underline{V} = \text{grad } \Phi) \ldots\ldots\ldots (1)$$

satisfies Laplace equation

Note.—Discussion open until October 1, 1972. To extend the closing date one month, a written request must be filed with the Executive Director, ASCE. This paper is part of the copyrighted Journal of the Waterways, Harbors and Coastal Engineering Division, Proceedings of the American Society of Civil Engineers, Vol. 98, No. WW2, May, 1972. Manuscript was submitted for review for possible publication on September 28, 1971.

[1] Grad. Asst., Hydraulics and Hydrodynamics Lab. and Dept. of Appl. Math., Technion, Israel Inst. of Technology, Haifa, Israel.

[2] Assoc. Prof., Hydraulics and Hydrodynamics Lab. and Dept. of Appl. Math., Technion, Israel Inst. of Technology, Haifa, Israel.

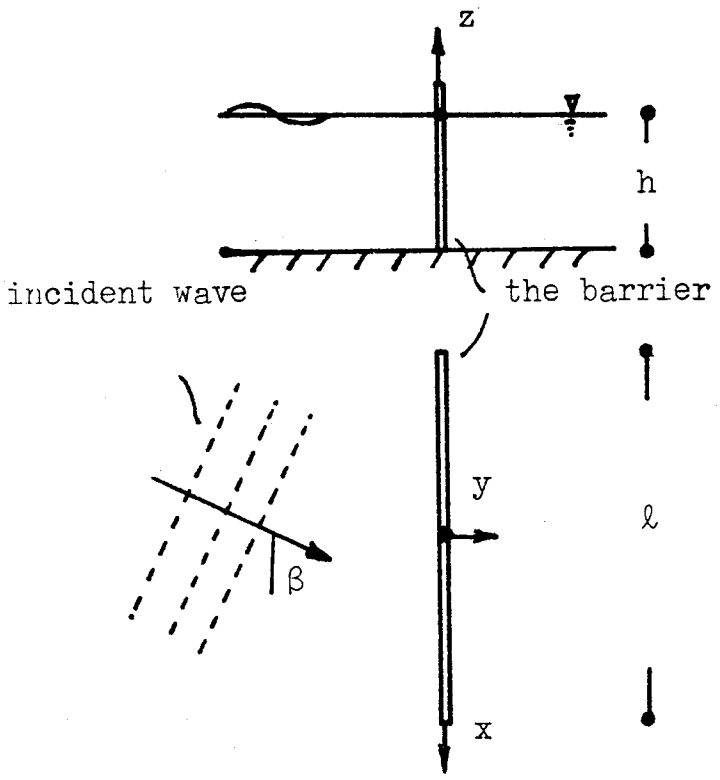

FIG. 1.—VERTICAL CROSS SECTION AND VIEW OF OBSTACLE AND INCIDENT WAVE

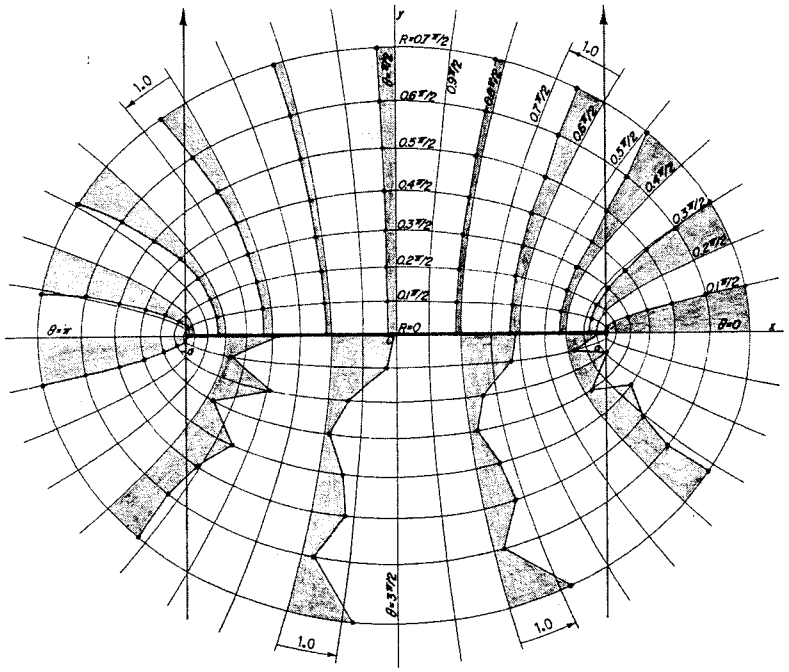

FIG. 2.—DIMENSIONLESS WAVE AMPLITUDE $\sqrt{EP/EP_0}$ NEAR OBSTACLE ($\beta = 90°$, $\lambda \neq l = 0.2$)

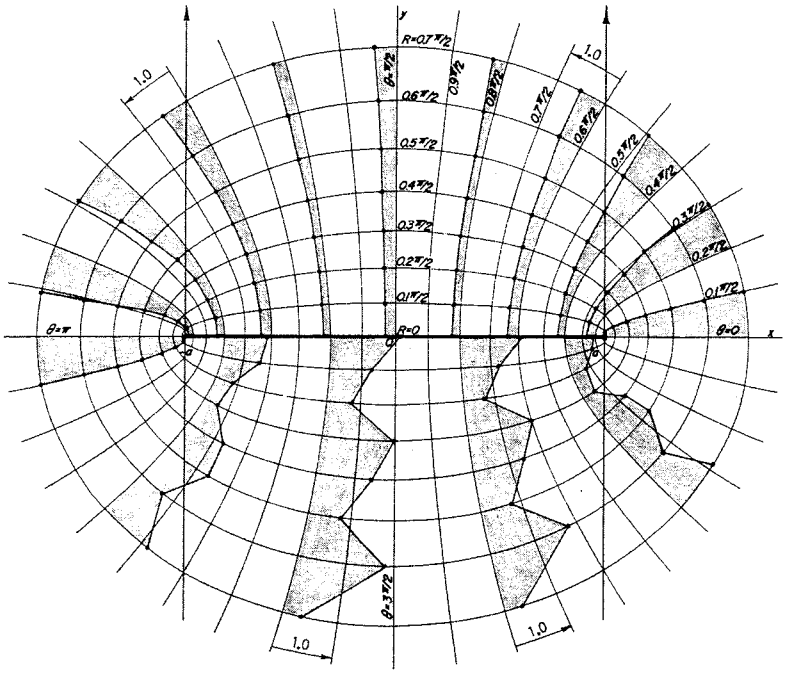

FIG. 3.—DIMENSIONLESS WAVE AMPLITUDE $\sqrt{EP/EP_0}$ NEAR OBSTACLE (β = 90°, λ/l = 0.5)

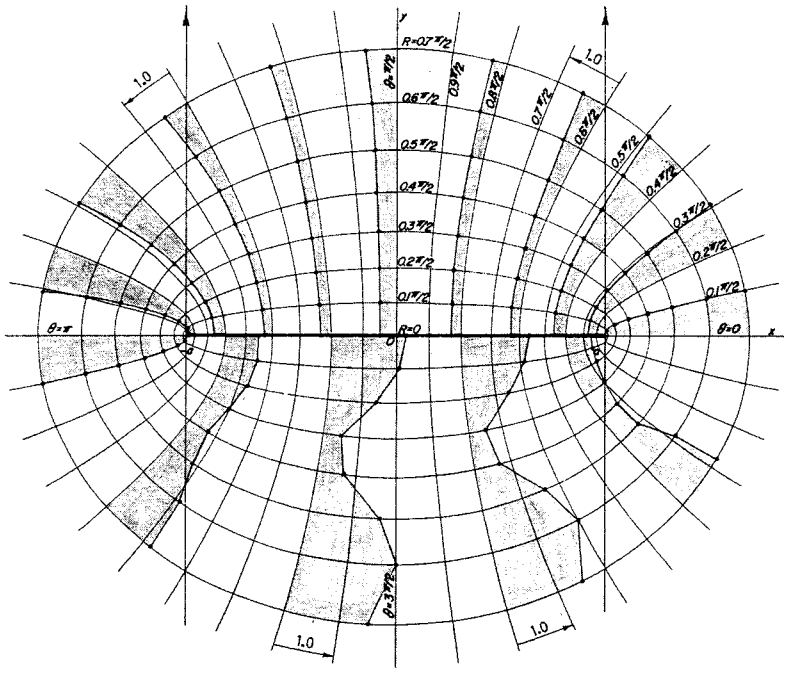

FIG. 4.—DIMENSIONLESS WAVE AMPLITUDE $\sqrt{EP/EP_0}$ NEAR OBSTACLE (β = 90°, λ/l = 1.0)

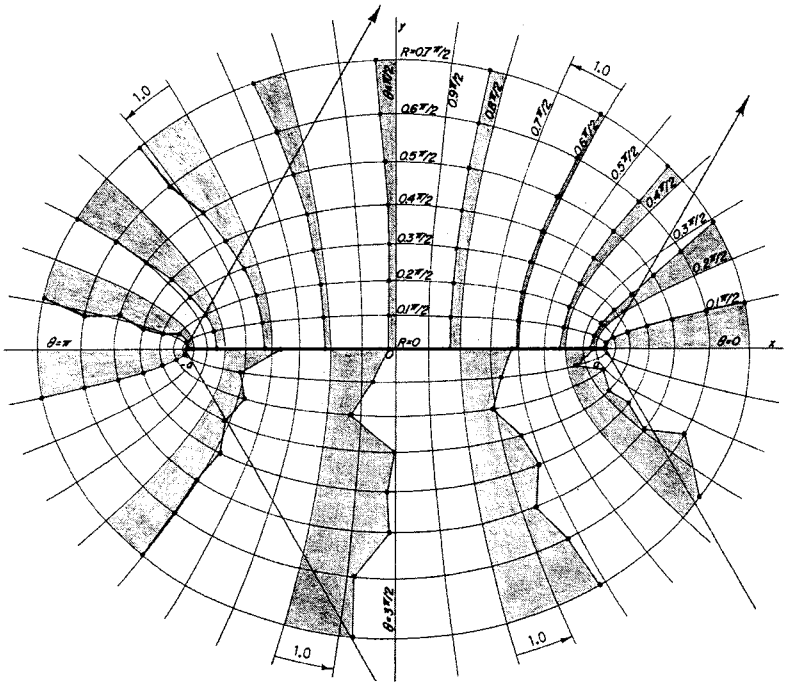

FIG. 5.—DIMENSIONLESS WAVE AMPLITUDE $\sqrt{EP/EP_0}$ NEAR OBSTACLE (β = 60°, λ/l = 0.2)

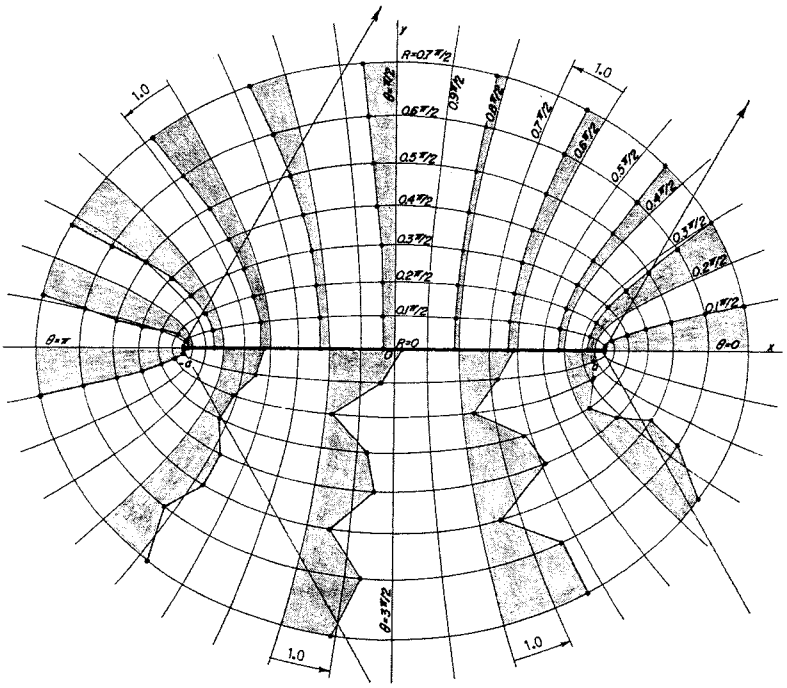

FIG. 6.—DIMENSIONLESS WAVE AMPLITUDE $\sqrt{EP/EP_0}$ NEAR OBSTACLE (β = 60°, λ/l = 0.5)

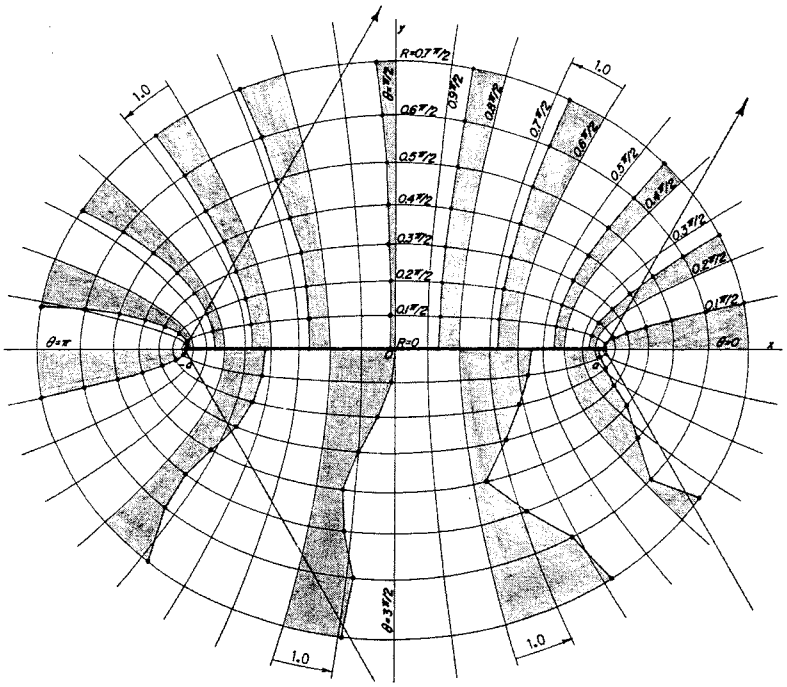

FIG. 7.—DIMENSIONLESS WAVE AMPLITUDE $\sqrt{EP/EP_0}$ NEAR OBSTACLE (β = 60°, λ/l = 1.0)

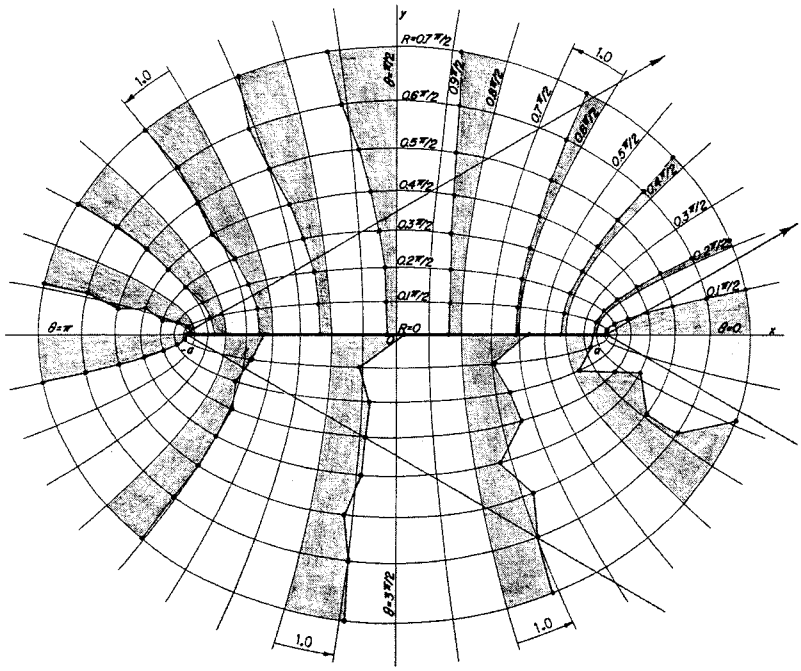

FIG. 8.—DIMENSIONLESS WAVE AMPLITUDE $\sqrt{EP/EP_0}$ NEAR OBSTACLE (β = 30°, λ/l = 0.2)

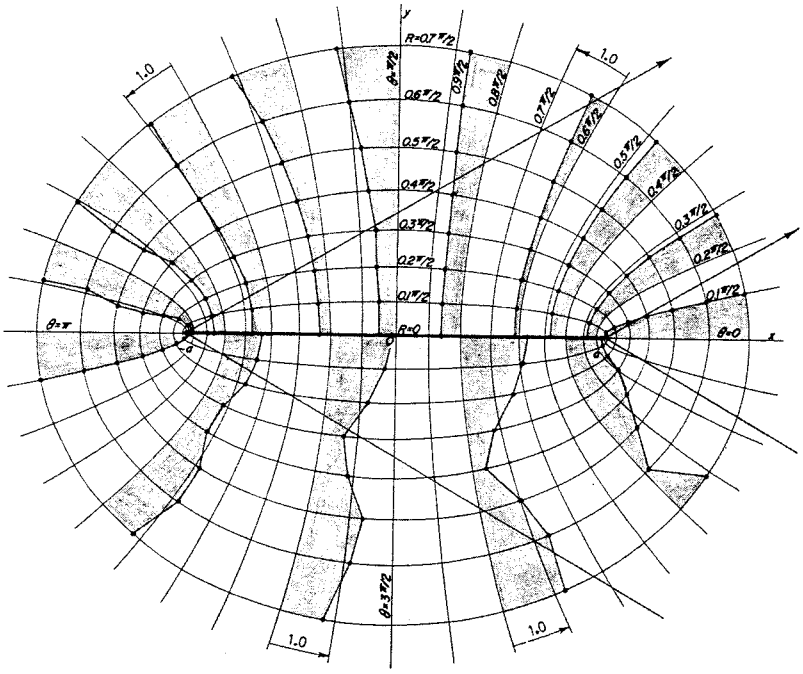

FIG. 9.—DIMENSIONLESS WAVE AMPLITUDE $\sqrt{EP/EP_o}$ NEAR OBSTACLE (β = 30°, λ/l = 0.5)

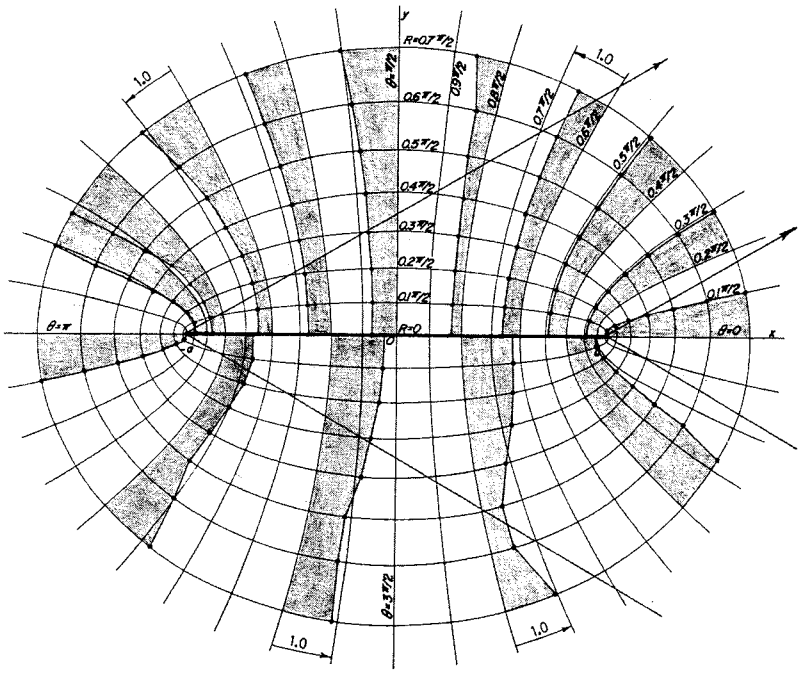

FIG. 10.—DIMENSIONLESS WAVE AMPLITUDE $\sqrt{EP/EP_o}$ NEAR OBSTACLE (β = 30°, λ/l = 1.0)

$$\nabla^2 \phi = 0 \quad \ldots\ldots (2)$$

in which x, y, z = cartesian coordinates; t = time; and ω = wave frequency.

The flow domain is of infinite extent in x, y directions and of finite constant depth. The barrier is characterized by its length l.

The boundary conditions satisfied by ϕ are as follows:

$$\phi_{,z} = 0 \quad (z = -h) \quad \ldots\ldots (3)$$

on the bottom and

$$\phi_{,z} - \sigma\phi = 0 \quad (z = 0); \quad \sigma = \frac{\omega^2}{g} \quad \ldots\ldots (4)$$

on the free-surface, after linearization.

The incident wave, attacking from infinity is described by

$$\phi^I = a\, f_1(z) \exp(ik_1\rho); \quad \rho = x \cos\beta + y \sin\beta \quad \ldots\ldots (5)$$

in which a = constant related to the wave amplitude; $k_1 = 2\pi/\lambda$ = wave number; λ = wave length; and $f_1(z)$ has the usual expression:

$$f_1(z) = \frac{\sqrt{2}\ \mathrm{ch}\,[k_1(z+h)]}{\left[h + \frac{1}{\sigma}\,\mathrm{sh}^2\,(k_1 h)\right]^{1/2}} \quad \ldots\ldots (6)$$

It is customary to represent ϕ as the sum of the incident and scattered wave potentials:

$$\phi = \phi^I + \phi^S \quad \ldots\ldots (7)$$

The solution is rendered unique by requiring that at infinity ϕ^S represents outgoing waves solely.

The last boundary condition, to be analyzed later, is the one prevailing along the obstacle.

GENERAL SOLUTION

First, the problem is reformulated in terms of elliptical coordinates (2,5), by using the transformation

$$x = \frac{l}{2} \cosh r \cos\theta \quad \ldots\ldots (8a)$$

$$y = \frac{l}{2} \sinh r \sin\theta \quad \ldots\ldots (8b)$$

$$z = z \quad \ldots\ldots (8c)$$

The obstacle contour has now the simple equation $r = 0$. Following Refs. 3 and 4, the variables are separated:

$$\phi^S = Z(z)\ \Theta(\theta)\ R(r) \quad \ldots\ldots (9)$$

and the general solution for ϕ (8) satisfying Eqs. 2, 3, and 4 is obtained as follows:

$$\phi = \phi^I + \sum_{m=0}^{\infty} \left[b^*_{m_1} f_1(z)\, Me_m^{(1)}(r, q_1)\, ce_m(\theta, q_1) \right.$$

$$+ \sum_{n=2}^{\infty} b^*_{mn} f_n(z) \, Fek_m(r, -q_n) \, ce_m(\theta, -q_n) \Bigg]$$

$$+ \sum_{m=1}^{\infty} \Bigg[b_{m_1} f_1(z) \, Ne_m^{(1)}(r, q_1) \, se_m(\theta, q_1)$$

$$+ \sum_{n=2}^{\infty} b_{mn} f_n(z) \, Gek_m(r, -q_n) \, se_m(\theta, -q_n) \Bigg] \quad \ldots\ldots\ldots\ldots \quad (10)$$

in which b^*_{m1}, b^*_{mn}, b_{m1}, and b_{mn} = unknown constants. The Mathieu functions appearing in Eq. 10 have been selected such that ϕ^S satisfies the radiation condition at infinity. The boundary conditions (Eqs. 3 and 4) are satisfied if

$$\left. \begin{aligned} f_n(z) &= \frac{\sqrt{2} \cos\left[\frac{4q_n^{1/2}}{l}(z + h)\right]}{\left[h - \frac{1}{\sigma}\sin^2\left(4q_n^{1/2}\frac{h}{l}\right)\right]^{1/2}} \\ (n &= 2, 3 \ldots) \end{aligned} \right\} \quad \ldots\ldots\ldots\ldots\ldots\ldots \quad (11)$$

while eigenvalues q_n fulfill conditions

$$\frac{4q_1^{1/2}}{l} \tanh\left(\frac{4q_1^{1/2}}{l} h\right) = \sigma; \quad \frac{4q_1^{1/2}}{l} = k_1 \quad \ldots\ldots\ldots\ldots\ldots\ldots \quad (12a)$$

$$\frac{4q_n^{1/2}}{l} \tan\left(\frac{4q_n^{1/2}}{l} h\right) = -\sigma; \quad n = 2, 3, \ldots \quad \ldots\ldots\ldots\ldots\ldots \quad (12b)$$

The incident wave may be also represented by a similar series (3) as follows:

$$\phi^I = 2a \, f_1(z) \sum_{m=0}^{\infty} \Bigg\{ Ce_{2m}(r, q_1) \, ce_{2m}(\beta, q_1) \, ce_{2m} \frac{(\theta, q_1)}{p_{2m}(q_1)}$$

$$+ Se_{2m+2}(r, q_1) \, se_{2m+2}(\beta, q_1) \, se_{2m+2} \frac{(\theta, q_1)}{s_{2m+2}(q_1)}$$

$$+ i \Bigg[Ce_{2m+1}(r, q_1) \, ce_{2m+1}(\beta, q_1) \, ce_{2m+1} \frac{(\theta, q_1)}{p_{2m+1}(q_1)}$$

$$+ Se_{2m+1}(r, q_1) \, se_{2m+1}(\beta, q_1) \, se_{2m+1} \frac{(\theta, q_1)}{s_{2m+1}(q_1)} \Bigg] \Bigg\} \quad \ldots\ldots\ldots\ldots \quad (13)$$

The unknown coefficients of Eq. 10 have now to be determined from the boundary condition on the obstacle.

IMPERVIOUS BARRIER

General.—The boundary condition along the obstacle becomes in this case

$$\phi_{,r} = 0 \quad (r = 0; \; -h \leq z \leq 0) \quad \ldots\ldots\ldots\ldots\ldots\ldots \quad (14)$$

From Eqs. 10, 13, and 14 and by using the orthogonality of the eigenfunctions in the z and θ directions

$$\int_{-h}^{0} f_i(z)\, f_j(z)\, dz = \delta_{ij} \quad \ldots\ldots\ldots\ldots\ldots\ldots\ldots\ldots \quad (15a)$$

$$\int_{0}^{2\pi} se_i(\theta, q)\, se_j(\theta, q)\, d\theta = \delta_{ij}\, \pi \quad \ldots\ldots\ldots\ldots\ldots\ldots\ldots \quad (15b)$$

the following values of the coefficients are immediately obtained:

$$b^*_{m1} = b^*_{mn} = b_{mn} = 0 \quad \ldots\ldots\ldots\ldots\ldots\ldots\ldots\ldots \quad (16a)$$

$$b_{(2m+1)1} = -\,2a\,i\,Se'_{2m+1}(0, q_1)\, se_{2m+1}\, \frac{(\beta, q_1)}{s_{2m+1}(q_1)\, Ne^{(1)'}_{2m+1}(0, q_1)} \quad (16b)$$

$$b_{(2m+2)1} = -\,2a\,Se'_{2m+2}(0, q_1)\, se_{2m+2}\, \frac{(\beta, q_1)}{s_{2m+2}(q_1)\, Ne^{(1)'}_{2m+2}(0, q_1)} \quad (16c)$$

Thus the complete expression of the velocity potential becomes, with the aid of Eqs. 1, 5, 10, and 16:

$$\left.\begin{aligned} \Phi &= a\, f_1(z)\, e^{-i\omega t}\left[e^{ik_1\rho} + \sum_{n=1}^{\infty}\left(\frac{b_m}{a}\right)_1 Ne^{(1)}_m(r, q_1) se_m(\theta, q_1)\right] \\ &= a\, f_1(z)\, e^{-i\omega t}\left[e^{ik_1\rho} + |\xi|\, e^{i\arg(\xi)}\right] \end{aligned}\right\} \quad (17a)$$

in which

$$\xi(\theta, r) = |\xi|^{i\arg(\xi)} = \sum_{n=1}^{\infty}\left(\frac{b_m}{a}\right)_1 Ne^{(1)}_m(r, q_1) se_m(\theta, q_1) \quad \ldots\ldots \quad (17b)$$

The free-surface elevation is given by

$$\left.\begin{aligned} \eta &= -\frac{1}{g}\left|\frac{\partial[\mathrm{Re}\,(\Phi)]}{\partial t}\right|_{z=0} \\ &= \frac{-\omega a}{g}\, f_1(0)\, \{\sin(k_1\rho - \omega t) + |\xi|\sin[\arg(\xi) - \omega t]\} \end{aligned}\right\} \quad \ldots \quad (18)$$

and the ratio between η and η_0 (- the incident wave amplitude) becomes

$$\frac{\eta}{\eta_0} = \sin(k_1\rho - \omega t) + |\xi|\sin[\arg(\xi) - \omega t] \quad \ldots\ldots\ldots\ldots \quad (19)$$

The potential energy of the waves results from the averaging of η^2 over a period. Therefore

$$\frac{\mathrm{EP}(\theta, r)}{\mathrm{EP}_0} = \frac{\overline{\eta^2}}{\frac{1}{2}\eta_0} = 1 + 2|\xi|\cos[\arg(\xi) - k_1\rho] + |\xi|^2 \quad \ldots\ldots \quad (20)$$

In the absence of the obstacle $\xi \equiv 0$ and $\mathrm{EP}(\theta, r)/\mathrm{EP}_0 \equiv 1$, as it should be. The solution given in this paragraph is analogous to that of the electromagnetic potential (5). There are, however, two significant differences between Ref. 5 and the present work: (1) While in the electromagnetic and acoustic theories one is interested mainly in the computation of the scattered wave far from the obstacle, herein it is of paramount importance to determine the state of the sea near the barrier, which is also a more difficult task; and (2) the range of

ratios λ/l has been extended in the present work below the minimum value $\lambda/l = 0.7$ considered in Ref. 5.

The potential Φ (Eq. 17) depends in a complex manner on the two parameters λ/l and β; h/l and η_o/l appear in a simple manner in the coefficient in front of the expression of Φ, in contrast with the case of a partially submerged obstacle. The ratio $\sqrt{EP/EP_o}$ (Eq. 20) has been computed for different points of the field for a few values of λ/l ($\lambda/l = 0.2$, 0.5, and 1.0) and β ($\beta = 30°$, 60°, and 90°).

In the extreme case of $\lambda/l \to 0$ the situation is similar to that of the geometrical optics and a complete shadow is created beyond the barrier. Conversely, for $\lambda/l \to \infty$ the obstacle behaves like a thin rod with little influence on the incident wave.

The computation of $\sqrt{EP/EP_o}$ (Eq. 20) has been carried out by using the Technion I.B.M. 360/50 computer. The values of the Mathieu functions have been determined with the aid of Refs. 1, 3, and 6; $\sqrt{EP/EP_o}$ has been computed for discrete points at the intersections of hyperbolas of constant θ ($\theta = 0, 0.2\pi/2, 0.4\pi/2, \ldots, \pi, 1.2\pi \ldots 2\pi$) and ellipses of constant r ($r = 0, 0.1\pi/2 \ldots, 0.7\pi/2$). The results are given in tables which may be found in Ref. 8. Herein the results are presented in a graphical compact form in Figs. 2 to 10.

Analysis of Results.—For $\beta = 90°$ (Figs. 2, 3, 4) the following conclusions seem appropriate: (1) The breakwater creates a relatively still zone in its shadow up to a distance of at least 2/3 of its length, normally to the axis; (2) the lateral influence of the barrier is negligible; (3) the waves are amplified upstream and they have the character of standing waves. Due to interference the amplitude may, however, be larger than twice the amplitude of the incident wave; and (4) although generally the magnitude of the wave energy along the downstream face decreases from the edges towards the center, the drop is not monotonical, due to interference effect. For $\beta = 60°$ (Figs. 5, 6, and 7) the same conclusions as for $\beta = 90°$ are qualitatively valid. In the case of $\beta = 30°$ (Figs. 8, 9, 10) the effectiveness of the barrier in creating a still zone is greatly reduced. In all cases the energy downstream decreases as λ/l decreases.

Comparison With Wiegel (9) Solution for Semi-Infinite Barrier.—Wiegel (9) has derived a solution for a semi-infinite barrier and has given maps for the state of the sea near the edge. The comparison with the present solution, which is valid for an obstacle of finite length, shows that for $\beta = 90°$ and $\lambda/l = 0.2$, the agreement between the two solutions is satisfactory up to two wave lengths from the edge, i.e., the interference between the two edges is weak in this zone. For $\beta < 90°$ the agreement becomes poor as β decreases and in fact it is difficult to separate the zones of influence of the two edges.

Comparison With Morse and Rubenstein (5) Solution.—The global coefficient of energy scattering

$$GC = \int_S |\xi|^2 \frac{dS}{2l} \quad \ldots\ldots\ldots\ldots\ldots\ldots\ldots\ldots\ldots\ldots\ldots\ldots\ldots\ldots\ldots\ldots\ldots\ldots \quad (21)$$

in which S = ellipse far from the obstacle, i.e., $r \to \infty$, has been also computed and compared with values found by Morse and Rubenstein (5) in the limited range of λ/l considered by them. The agreement being excellent it was concluded that the numerical computations are quite accurate. The values of GC may be found in Ref. 8, but they are of a minor significance in the case of water waves.

Review of Montefuso Work.—Montefuso (1968) has carried out an analysis of the wave diffraction by an impervious breakwater. The present work supplements, however, his results rather than duplicating them.

Montefuso has solved the problem for ratios $\lambda/l > 0.57$ where herein the smallest $\lambda/l = 0.2$. The small ratio is particularly interesting in the case of long breakwaters encountered frequently in applications. Moreover, the computations are more elaborate in the latter case.

More important, the maps of the wave energy presented by Montefuso do not cover the region in the vicinity of the breakwater, while Figs. 2 to 10 give the detailed picture in the neighborhood of the obstacle. Thus, the two types of maps supplement each other in describing the state of the sea around the breakwater.

PERVIOUS BREAKWATER

To acquire some information on the influence of the permeability of the breakwater's body upon the wave transformation it was assumed that (1) There is no storage (consistent with the neglection of the thickness); and (2) the resistance to the flow through the obstacle is linear in the velocity (Darcy's law). Thus

$$V(z, \theta = \alpha, r = 0) = V(z, \theta = -\alpha, r = 0) \quad \ldots\ldots\ldots\ldots \quad (22a)$$

$$V = \frac{K}{B}\left[\left(\frac{P}{\gamma} + z\right)\Big|_{\theta=-\alpha} - \left(\frac{P}{\gamma} + z\right)\Big|_{\theta=\alpha}\right] \quad r = 0 \quad \ldots\ldots\ldots\ldots \quad (22b)$$

in which K = hydraulic conductivity coefficient in Darcy's law and B = width of the breakwater. From Eq. 22 the following conditions are obtained:

$$\phi_{,r}(z, \theta = \alpha, r = 0) = -\phi_{,r}(z, \theta = -\alpha, r = 0) \quad \ldots\ldots\ldots \quad (23a)$$

$$\frac{\phi_{,r}(z, \theta = \alpha, r = 0)}{0.5l} \sin \alpha = \frac{i\omega K}{gB}\left[\phi(z, \theta = -\alpha, r = 0)\right.$$

$$\left. - \phi(z, \theta = \alpha, r = 0)\right] \quad \ldots\ldots\ldots\ldots\ldots\ldots\ldots\ldots \quad (23b)$$

The solution for ϕ in this case is still represented by Eq. 10. Also $b^*_{mn} = 0$ and Eq. 23*b* is replaced by

$$\phi^I_{,r}(z, \theta, r = 0) = -\phi^S_{,r}(z, \theta, r = 0)$$

$$- \frac{i\omega l K}{gB} \sin \Theta \, \phi^S(z, \Theta, r = 0) \quad \ldots\ldots\ldots\ldots\ldots\ldots\ldots \quad (24)$$

Multiplying Eq. 24 by $f_n(z) \sin m\theta$, integrating along z and θ and using the properties of $f_n(z)$ and Mathieu functions, one may obtain a linear system of equations for the unknown coefficients b_{mn}. This system is infinite but may be solved approximately by truncation. As the purpose of the computations of this section is to reach qualitative results, it was assumed somewhat artificially that the ratio K/B varies along the barrier as

$$\frac{K}{B} = \frac{K_o}{B_o} \sin \theta \quad \ldots\ldots\ldots\ldots\ldots\ldots\ldots\ldots\ldots\ldots \quad (25)$$

i.e., the breakwater is less pervious at its center than at its edges. For this

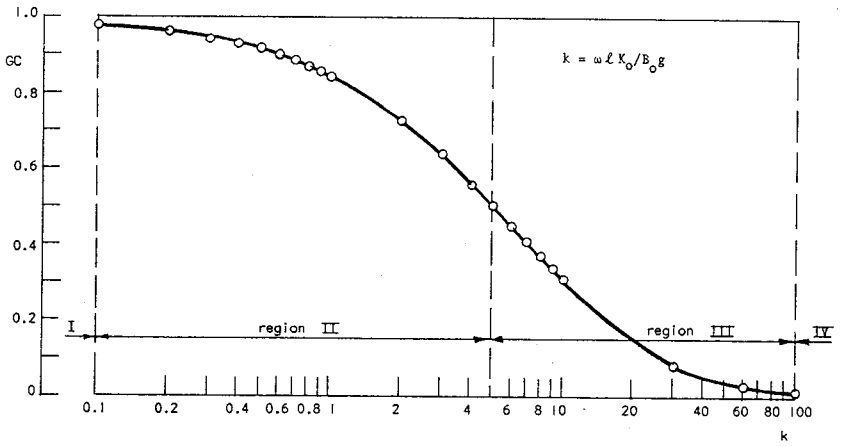

FIG. 11.—INFLUENCE OF DIMENSIONLESS PERMEABILITY COEFFICIENT k ON SCATTERING COEFFICIENT GC FOR PERMEABLE BREAKWATER (λ/l = 0.2, β = 90°)

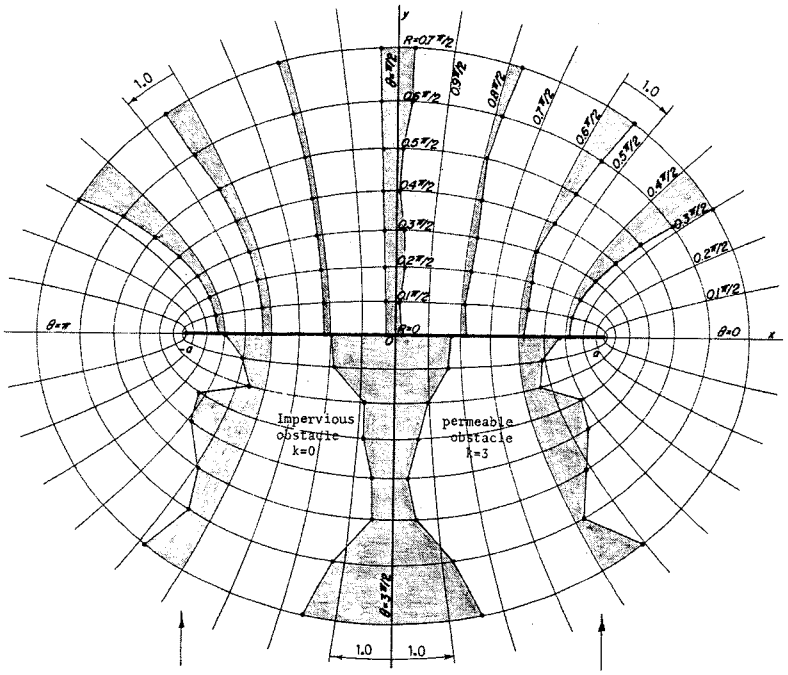

FIG. 12.—COMPARISON BETWEEN WAVE AMPLITUDE $\sqrt{EP/EP_0}$ NEAR PERVIOUS AND IMPERVIOUS OBSTACLE (β = 90°, λ/l = 0.2)

particular case the coefficients are obtained at once as follows:

$$b_{mn} = 0; \ (n \geq 2, \ m \geq 1) \quad \ldots\ldots\ldots\ldots\ldots\ldots\ldots\ldots \quad (26a)$$

$$b_{(2m+2)1} = -\, 2a\, Se'_{(2m+2)}(0, q_1)\, \frac{se_{(2m+2)}(\beta, q_1)}{s(q_1)_{(2m+2)}} \left[ikNe^{(1)}_{(2m+2)}(0, q_1)\right.$$

$$\left. + Ne^{1'}_{(2m+2)}(0, q)\right]; \ (m \geq 0) \quad \ldots\ldots\ldots\ldots\ldots\ldots\ldots\ldots \quad (26b)$$

$$b_{(2m+1)1} = -2ia\, Se'_{(2m+1)}(0, q_1)\frac{se_{(2m+1)}(\beta, q_1)}{s_{(2m+1)}(q_1)}\,[ikNe^1_{(2m+1)}(0, q_1)$$

$$+ Ne^{1\,\prime}_{(2m+1)}(0, q_1)]; \quad (m \geq 0) \qquad (26c)$$

Eqs. 26 are a generalization of the solutions for an impervious breakwater (Eq. 16), the additional dimensionless parameter being

$$k = \frac{\omega l K_o}{B_o g} \qquad (27)$$

Term k has the character of a damping coefficient for a linear oscillator. For $k = 0$ the solution for an impervious barrier is recovered, while for $k \to \infty$ the obstacle vanishes.

To study the influence of the magnitude of k, computations have been carried for $\beta = 90°$, $\lambda/l = 0.2$, and different k values.

The variation of the global coefficient of energy scattering with k is given in Fig. 11. The transition from an impervious obstacle ($k = 0$) to the pure incident wave ($k = \infty$) is clearly seen in this figure. The wave energy distribution near the barrier has been computed for a few values of k. An example is given in Fig. 12 in which the map of $\sqrt{EP/EP_o}$ for $k = 3$ is compared with that of an impervious obstacle ($k = 0$). The detailed analysis suggests the following characteristic ranges of k values: (1) $k = 0/0.1$, the obstacle is practically impervious; (2) $k = 0.1/5$, the wave energy is reduced in the upstream zone, but very little in the shadow of the barrier, as compared with the impervious obstacle; (3) $k = 5/100$, the wave energy in front of the barrier is further reduced, while in the downstream region the waves become higher than those prevailing behind an impervious barrier; and (4) $k > 100$, the influence of the obstacle becomes negligible. All these effects may be explained by the energy losses occuring in a pervious breakwater, as well as by changes in the interference pattern.

Concluding, the optimal range of k is that of range (2). For such values the breakwater operates almost as well as an impervious one in creating a still zone behind it, but reduces the energy of the waves in front of it. Attention has to be paid to the fact that k incorporates the breakwater properties as well as the wave frequency.

EXTENSION TO RANDOM SEA

The random incident waves are assumed to obey the stochastic model proposed by Pierson (7):

$$\frac{\eta^I(x, y, t)}{\eta_o} = \int_{\lambda_1}^{\lambda_2}\int_{\beta_1}^{\beta_2} \sin\left[\frac{2\pi\rho}{\lambda} - \omega(\lambda)t + \epsilon(\lambda, \beta)\right]\sqrt{A^2(\lambda, \beta)\,d\lambda d\beta} \qquad (28)$$

in which $A^2(\lambda, \beta)$ = the energy spectrum. The random phase shift $\epsilon(\lambda, \beta)$ has a rectangular distribution in the range $(-\pi, \pi)$ and the model represents a multivariate Gaussian process stationary in three variables x, y, t. It may be shown that in the presence of the obstacle

$$\frac{\eta(x, y, t)}{\eta_o} = \int_{\lambda_1}^{\lambda_2}\int_{\beta_1}^{\beta_2} \left\{\sin\left(\frac{2\eta\phi}{\lambda} - \omega t + \epsilon\right)\right.$$

$$+ |\xi| \sin [\arg(\xi) - \omega t + \epsilon)] \sqrt{A^2(\lambda,\beta)\, d\lambda d\beta} \Big\} \quad \ldots\ldots\ldots\ldots \quad (29)$$

in which $\xi(x,y,\lambda,\beta)$ is given by Eq. 17*b*. Similarly, the dimensionless average potential energy is given by

$$\frac{\overline{EP(r,\theta)}}{EP_o} = \frac{\overline{\eta^2}^{\text{sample}}}{\frac{1}{2}\eta_o^2} = \int_{\lambda_1}^{\lambda_2}\int_{\beta_1}^{\beta_2} \left\{1 + 2|\xi| \cos\left[\arg(\xi) - \frac{2\pi\rho}{\lambda}\right] + |\xi|^2\right\} A^2(\lambda,\beta)\, d\lambda d\beta$$

$$= \int_{\lambda_1}^{\lambda_2}\int_{\beta_1}^{\beta_2} \left\{\frac{EP(r,\theta,\lambda,\beta)}{EP_o}\right\} A^2(\lambda,\beta)\, d\lambda d\beta \quad \ldots\ldots \quad (30)$$

in which EP_o = energy of an arbitrary monochromatic wave. Eq. 30 shows that the average energy at a point is obtained by integrating the energies of the spectrum components. Eq. 30 as well as the fact that the sea state is represented by a multivariate Gaussian process stationary in t, in the presence of the obstacle, are proved in Ref. 8.

As an example, energy EP/EP_o has been computed in the case of an impervious barrier at point A($r = 0.1\pi$, $0 = 0.5\pi$) in Fig. 13, for a band of $0.3 < \lambda/l < 0.5$. The undulating nature of the curve of Fig. 13 clearly indicates the interference effects of the obstacle edges.

In addition the wave average energy at the same point, $(\overline{EP}/EP_o)$ has been computed by integrating Eq. 30 with a constant spectrum $A^2(\lambda,\beta)$ in the band $0.3 < \lambda/l < 0.5$ and for $\beta = 90°$, as it is appropriate near the coast. Taking EP_o as the total energy contained in the spectrum of the incident waves, $\overline{EP}/EP_o$ (Eq. 30) was found to be equal to 0.170. Assuming a monochromatic deterministic incident wave with $\lambda/l = 0.4$ (the average wavelength in the con-

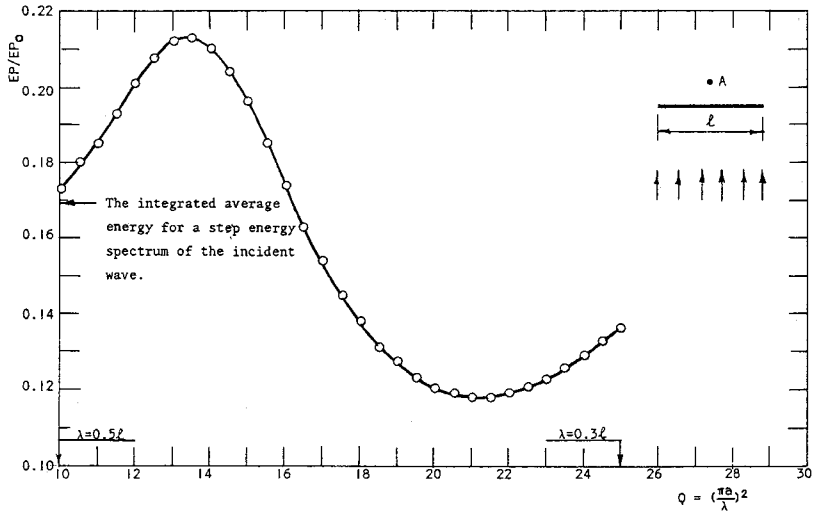

FIG. 13.—DISTRIBUTION OF WAVE ENERGY EP/EP_o BEHIND THIN BARRIER AS FUNCTION OF WAVE LENGTH AT POINT A($r = 0.1\pi$, $\theta = 0.5\pi$)

sidered band) and with the same total energy EP_o, the value of EP/EP_o (Eq. 20) = 0.185. Thus, in the particular case considered herein the replacement of the random incident wave with a narrow wavelength band by a monochromatic wave results in a small error.

CONCLUSIONS

By using elliptical coordinates, an efficient method of computing the wave energy distribution near a thin detached breakwater has been set forth. The detailed maps of the sea state near the obstacle provide the necessary data for the evaluation of the breakwater performance at different wave length and angles of attack.

The qualitative analysis of the influence of the permeability of the breakwater body indicates the optimal range of the permeability values for given waves. The analysis is of a little quantitative value because of the nonlinearity of the resistance of the breakwater body which prevails in most applications.

ACKNOWLEDGMENT

The present work is part of a thesis by M. Stiassnie, submitted to the Dept. of Applied Math., Technion, as partial fulfillment of the requirements for a Masters of Science degree.

APPENDIX I.—REFERENCES

1. Blanch, G., "On the Computation of Mathieu Functions," *Journal of Mathematical Physics*, Vol. 25, 1946, pp. 1–20.
2. Carr, J. H., and Marshall, E. S., "Diffraction of Water Waves by Breakwater," *Circular 521*, National Bureau of Standards, 1952, pp. 109–125.
3. McLachlan, N. W., "Theory and Application of Mathieu Functions," Dover Publications, 1964.
4. Montefuso, L., "The Diffraction of a Plane Wave by an Isolated Breakwater," *Meccanica*, Vol. 3, 1968, pp. 156–166.
5. Moon, P., and Spencer, D. E., "Field Theory Handbook," Springer-Verlag, 1961.
6. Morse, P. M., and Rubenstein, P. J., "The Diffraction of Waves by Ribbons and Slits," *Physical Review*, Vol. 54, 1938, pp. 895–898.
7. Pierson, W. J., "Wind-Generated Gravity Waves," *Advances in Geophysics*, Vol. 2, 1955, pp. 93–178.
8. Stiassnie, M., "Scattering of Gravity Waves by Elliptical Obstacles," thesis presented to the Israel Institute of Technology, at Haifa, Israel, in 1971, in partial fulfillment of the requirements for the degree of Master of Science. (In Hebrew with English summary).
9. "Tables Relating to Mathieu Functions," National Bureau of Standards, Applied Mathematics Series, No. 59, 1967.
10. Wiegel, R. L., "Diffraction of Waves by Semi-Infinite Breakwater," *Transactions*, ASCE, Vol. 128, Part I, Paper No. 3477, 1963, pp. 1181–1202.

APPENDIX II.—NOTATION

The following symbols are used in this paper:

$A^2(\lambda, \beta)$ = energy spectrum;
a = constant related to wave's amplitude;
B, B_o = width of breakwater;
b_{mn}, b^*_{mn} = coefficients;
$ce_m(\theta, q)$, $Ce_m(r, q)$ = Mathieu function, see Ref. 3;
EP = potential wave energy;
$\overline{\text{EP}}$ = average potential wave energy;
EP_o = potential energy of incident wave;
$Fek_m(r, q)$, $GeK_m(r, q)$ = Mathieu functions, see Ref. 3;
$f_n(z)$ = eigenfunctions in z direction;
GC = global scattering coefficient;
h = water depth;
K, K_o = hydraulic conductivity coefficient in Darcy's law;
k = dimensionless coefficient, see Eq. 27;
k_1 = wave number of incident wave;
l = breakwater's length;
m, n = integers;
$p_m(q)$, $p'_m(q)$ = constants, see Ref. 3;
$q_1, -q_n$ = eigenvalues in z direction;
r = elliptical coordinate;
$s_m(q)$, $s'_m(q)$ = constants, see Ref. 3;
$se_m(\theta, q)$, $Se_m(r, q)$ = Mathieu functions, see Ref. 3;
t = time;
V = velocity;
x, y, z = Cartesian coordinates;
β = incident wave angle of attack;
ϵ = random phase shift;
η = water surface elevation;
η^I = idem for incident wave;
η_o = incident wave's amplitude;
θ = elliptical coordinate;
λ = wave length;
ξ = see Eq. 17*b*;
ρ = see Eq. 5;
σ = see Eq. 4;
ϕ, Φ = potential function;
ϕ^I = potential of incident wave;
ϕ^S = potential of scattered wave; and
ω = wave frequency.